Experimental Generation of Spin-Photon Entanglement in Silicon Carbide

Ren-Zhou Fang,[1,2,3,*] Xiao-Yi Lai,[1,2,3,*] Tao Li,[1,2,3] Ren-Zhu Su,[1,2,3] Bo-Wei Lu,[1,2,3] Chao-Wei Yang,[1,2,3] Run-Ze Liu,[1,2,3] Yu-Kun Qiao,[1,2,3] Cheng Li,[4] Zhi-Gang He,[4] Jia Huang,[5] Hao Li,[5] Li-Xing You,[5] Yong-Heng Huo,[1,2,3] Xiao-Hui Bao,[1,2,3] and Jian-Wei Pan[1,2,3]

[1]*Hefei National Research Center for Physical Sciences at the Microscale and School of Physical Sciences, University of Science and Technology of China, Hefei 230026, China*

[2]*CAS Center for Excellence in Quantum Information and Quantum Physics, University of Science and Technology of China, Hefei 230026, China*

[3]*Hefei National Laboratory, University of Science and Technology of China, Hefei 230088, China*

[4]*National Synchrotron Radiation Laboratory, University of Science and Technology of China, Hefei, Anhui 230029, China*

[5]*State Key Laboratory of Materials for Integrated Circuits, Shanghai Institute of Microsystem and Information Technology, Chinese Academy of Sciences, 865 Changning Road, Shanghai 200050, China*

(Received 29 November 2023; accepted 20 March 2024; published 15 April 2024)

A solid-state approach for quantum networks is advantageous, as it allows the integration of nanophotonics to enhance the photon emission and the utilization of weakly coupled nuclear spins for long-lived storage. Silicon carbide, specifically point defects within it, shows great promise in this regard due to the easy of availability and well-established nanofabrication techniques. Despite of remarkable progresses made, achieving spin-photon entanglement remains a crucial aspect to be realized. In this Letter, we experimentally generate entanglement between a silicon vacancy defect in silicon carbide and a scattered single photon in the zero-phonon line. The spin state is measured by detecting photons scattered in the phonon sideband. The photonic qubit is encoded in the time-bin degree of freedom and measured using an unbalanced Mach-Zehnder interferometer. Photonic correlations not only reveal the quality of the entanglement but also verify the deterministic nature of the entanglement creation process. By harnessing two pairs of such spin-photon entanglement, it becomes straightforward to entangle remote quantum nodes at long distance.

DOI: 10.1103/PhysRevLett.132.160801

The hybrid entanglement between a matter qubit and a single photon serves as a fundamental resource for constructing quantum networks [1,2], opening the door to remarkable applications such as distributed quantum computing and long-distance quantum communication through the use of quantum repeaters [3]. To enable the practical implementation of these applications, it is crucial that the matter-photon entanglement exhibits both high efficiency and long coherence times [4,5]. The efficiency directly impacts the rate at which remote entanglement can be established, while the coherence time of the matter qubit determines the scalability of the system as the number of nodes increases. Solid-state systems [6] offer several advantages in this regard. Nanoscale cavities [7] can be built around matter qubits in order to significantly enhance the photon emission rate. Additionally, nuclear spins that couple weakly with environmental fields can be utilized for long-lived storage.

One promising avenue for realizing these goals is the exploration of optically active defects. Extensive research has been conducted on color centers in diamond [8–14], leading to significant progress in demonstrating key components and functionalities for quantum networks. However, there is a growing desire to go beyond diamond and explore alternative host materials [15–17] that are more cost-effective and amenable to nanofabrication. In recent years, defects in silicon carbide (SiC) have garnered significant interest [18]. Silicon carbide offers the advantages of large-scale, high-quality wafers that are already well-established in industry, as well as the feasibility of fabricating nanophotonic structures [19]. Preliminary studies have successfully identified stable optical transitions [20,21], initiated and manipulated electron spins and nuclear spins [20,22,23], generated indistinguishable photons [24], and demonstrated the feasibility of integration with nanophotonics [25–28], long-lived storage and single-shot readout via charge state control [29]. However, the realization of the essential element of spin-photon entanglement still remains to be achieved, which requires the integration of various SiC techniques on single impurities into a single experiment, and the adoption of single-photon techniques including filtering, interfering, and making correlation measurements.

In this Letter, we report the experimental generation of spin-photon entanglement in SiC. We make use of the V1-type silicon vacancy (V_{Si}) in the epilayer of a 4H-SiC wafer that is created via high-energy electron irradiation [30].

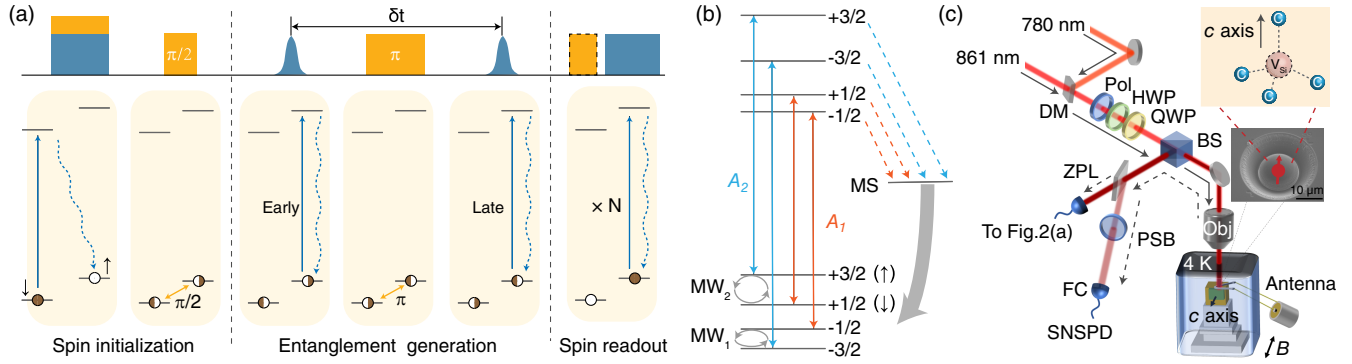

FIG. 1. Experimental scheme and setup. (a) Experimental sequence consisting of spin initialization, entanglement generation, and readout. (b) Energy level diagram of V1 centers. An external magnetic field parallel to the c axis lifts the degeneracy in ESs and GSs. Optical transitions A_1 and A_2, as well as spin transitions using MW_1, and MW_2, are present. We use $|+3/2\rangle_g$ as $|\uparrow\rangle$ state and $|+1/2\rangle_g$ as $|\downarrow\rangle$ state in the experimental protocol. Optical transitions with spin flip occur through the metastable state (MS), which involves phonons and optical spontaneous emission. (c) Experimental setup. FC, fiber coupler; BS, beam splitter; Pol, polarizer; HWP, half-wave plate; QWP, quarter-wave plate.

The defect has very narrow optical transitions that enable us to initialize the electron spin with a high fidelity via resonant optical pumping. By employing a time-bin entangling scheme, we are able to create the entanglement between the single photon's temporal modes and the electron spin. We make use of a stabilized unbalanced Mach-Zehnder (MZ) interferometer to measure the photonic qubit. We use photon corrections to characterize the entanglement quality. In comparison with other solid-state impurities, such as NV centers in diamond, the entanglement reported here with SiC is very promising for the future integration with nanophotonic, since high-quality wafer-scale SiC material is easily available and nanophotonic fabrication on SiC is mature [19,26].

Our experimental scheme shown in Fig. 1(a), and the V1 defect has an energy level diagram shown in Fig. 1(b) with a magnetic field in the c axis. With $S = 3/2$, both the ground and excited state have four sublevels, resulting in four optical transitions $|m_s\rangle_g \leftrightarrow |m_s\rangle_e$, with $m = 1/2, -1/2, 3/2, -3/2$. To form a qubit, we select two out of the four ground states' sublevels, defining $|\uparrow\rangle = |+3/2\rangle_g$ and $|\downarrow\rangle = |+1/2\rangle_g$. Since the g factor is identical for the ground states (GSs) and excited states (ESs), the four transitions are separated into two categories, with A_1 denoting the category $|\pm 1/2\rangle_g \leftrightarrow |\pm 1/2\rangle_e$, and A_2 denoting the category $|\pm 3/2\rangle_g \leftrightarrow |\pm 3/2\rangle_e$. The frequency difference between A_1 and A_2 is about 966 MHz due to the difference of zero-field splitting between the GSs and ESs.

To generate the desired spin-photon entangled state, we first initialize the defect to $|\uparrow\rangle$ and rotate it to a superpositional state of $(|\uparrow\rangle + |\downarrow\rangle)/\sqrt{2}$ via applying a microwave $\pi/2$ pulse. Afterward, we apply fast optical excitation for $|\uparrow\rangle$ and collect its photon emission. Then we add a microwave π pulse and apply the fast optical excitation and emission collection again. A single photon may be created either during the first or the second excitation step, thus generating a pair of spin-photon entanglement in the form of $|\Psi\rangle = (1/\sqrt{2})(|\uparrow\rangle|L\rangle + |\downarrow\rangle|E\rangle)$, where $|E\rangle$ denotes an early photon and $|L\rangle$ denotes a late photon. Please note that similar schemes have been adopted in previous experiments with NV centers [31] and quantum dots [32]. The correlations between the spin and photon states are measured in different basis by performing spin state projection and readout.

Our experimental setup is illustrated in Fig. 1(c). The SiC sample is placed in a cryogen-free cryostat operated at 4 K. We make use the laser at 861 nm for resonant excitation and 780 nm for off-resonant excitation. The 861 nm laser is actively stabilized with an ultrastable cavity to improve its phase coherence. The combined laser beams are focused on the sample with an objective (Obj) lens of NA = 0.65. Photon signal emitted from the sample is extracted through the reflection path of the 90:10 BS. To improve the photon collection efficiency, we fabricate a solid immersion lens (SIL) around the defect via focused ion beam milling. Fluorescence at 861 nm is recognized as the zero-phonon line (ZPL) emission, while fluorescence above 861 nm is recognized as the phonon sideband (PSB) emission [30]. In our experiment, we use a long-pass filter with an edge wavelength of 875 nm to split the ZPL and PSB. In addition we a bandpass filter (855–865 nm) on the ZPL path to reject noise.

To implement the spin-photon entanglement scheme, it is crucial for the color center to have excellent coherence both for the spin and the optical transitions. In the Supplemental Material [30], we perform detailed characterization for the optical transition linewidth, spin transition frequency, Rabi oscillation, and spin coherence time. These results provide a solid foundation for our experiment of spin-photon entanglement. Selecting the ZPL emission is crucial for quantum network applications, since photons emitted from distant nodes needs to be highly indistinguishable to get remote nodes entangled. As

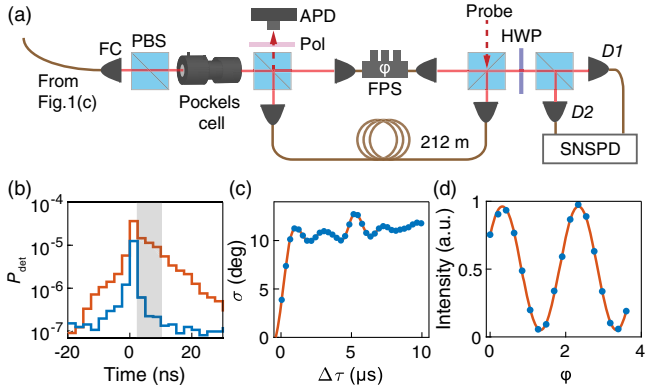

FIG. 2. Measurement of the ZPL photon. (a) Unbalanced MZ interferometer for verification of entanglement in the time-bin degree. The input is from the fiber-coupled ZPL signal in Fig. 1(c) PBS, polarizing beam splitter. (b) A histogram of the detection probability of ZPL and noise with the 10 ns detection window (gray region). The orange line represents the total signal. The noise is quantified by utilizing a 5 GHz detuned laser (blue line). P_{det}, detection probability. (c) Measurement of the laser phase noise at different time. The standard deviation σ is 11° with $\Delta\tau = 1.06$ μs for this experiment. (d) Visibility fringes of the imbalanced interferometer.

the ZPL has the same frequency with the resonant laser for excitation, frequency filtering, as used for PSB, does not work. In our experiment, we make use of polarization filtering and temporal filtering instead. We utilize a cross-polarization scheme [33,34]. The excitation and detection polarization are perpendicular to each other and both at $\theta = 45°$ relative to the fluorescence polarization. Scattered light from the curved surface of SIL has varying polarization at different positions, and the vibration from the cold head leads to random drifting of the sample position, resulting in the extinction ratio dropping to 30 dB. The optical excitation π pulse is made as short as 1 ns by using a fiber amplitude modulator together with a home-built electrical fast-pulse generator. A typical ZPL signal is shown in Fig. 2(b) with a bin width of 2.5 ns. The excitation π pulse opens in the $t = 0$ time bin. We apply a temporal window from $t = 2.5$ ns to $t = 12.5$ ns to filter out the ZPL signal. The ZPL signal is over 30 times higher than the sum of the background contribution, including laser photons, dark count, and after-pulse from the superconducting nanowire single photon detector (SNSPD).

To evaluate the spin-photon entanglement quality, we need to perform correlation measurements, which require measuring both the photon and the spin in various bases. To measure the time-bin encoded ZPL photon, we adopt an unbalanced MZ interferometer, as showed in Fig. 2(a). The Pockels cell directs the early photon to the long arm and late photon to the short arm, so the time-bin degree is converted to the polarization degree, i.e., $|E\rangle$ to $|V\rangle$ and $|L\rangle$ to $|H\rangle$. The relative time delay between the two arms matches the time difference of 1060 ns between the early and late mode to accommodate a π MW_2 pulse of 920 ns. Preserving the relative phase φ between the two optical modes is crucial for the measurements in the superpositional bases. Since the phase fluctuations of the 861 nm laser affect the coherence between early and late photons, we first measure the phase noise of the 861 nm laser using another unbalanced MZ interferometer with 5 μs delay between two arms (not shown) [35]. The phase evolution result is shown in Fig. 2(c). By calculating $\varphi(\tau_0) - \varphi(\tau_0 + \Delta\tau)$, we can analyze the phase shift of the laser and deduce the standard deviation of σ being 11° with $\Delta\tau = 1.06$ μs. In addition, we need to keep the relative phase between two arms of the interferometer stable. In Fig. 2(a), a probe beam with orthogonal polarization to the signal is introduced, following the same path as the signal. The phase information is converted into an intensity signal and detected by a sensitive avalanche photodiode (APD). Relative phase variations are compensated for by the proportional-integral-derivative circuit and a fiber piezo stretcher (FPS) on the short arm. To test the interferometer's phase stability, we send a 1 ns resonant laser pulse with different phase set point. As shown in Fig. 2(d), the interference visibility is 90%, which leads to a reduction in the measured visibility of the superpositional basis. The imperfection of the visibility arises from the rapid fluctuations of the phase, which exceed the bandwidth of the FPS.

The spin qubit is measured by detecting the PSB signal under resonant excitation. Under A_2 illumination, the PSB signal is proportional to the sum population in $|\pm 3/2\rangle_g$. Since our spin qubit is encoded in the subspace of $|\uparrow\rangle$ and $|\downarrow\rangle$, we can still use A_2 illumination to measure $|\uparrow\rangle$, and use MW_2 π pulse following A_2 illumination to measure $|\downarrow\rangle$. The duration of this measurement is typically set to 1 μs. Longer duration is unfavorable, as spin flip between $|\pm 1/2\rangle_g$ and $|\pm 3/2\rangle_g$ will happen and stop emitting photons. Measurement in a superpositional basis is performed by adding microwave rotations before the PSB detection.

Finally we conduct the experiment of spin-photon entanglement generation with the control pulses set as in Fig. 1(a). The spin is initialized to $|\uparrow\rangle$ with a fidelity of 96% via optical pumping. In order to characterize the entanglement quality, we measure the coincidence counts on the eigenbasis and superpositional basis between the ZPL signal created in the entanglement generation phase and the PSB signal in the spin readout phase. For measurements in the eigenbasis, the spin is projected to $|\uparrow\rangle$ or $|\downarrow\rangle$, the photon is projected to $|H\rangle$ or $|V\rangle$. While in the superpositional basis, the spin is projected to the states $|\pm\rangle = 1/\sqrt{2}(|\uparrow\rangle \pm |\downarrow\rangle)$, and the photon is projected to $|\pm\rangle = 1/\sqrt{2}(|H\rangle \pm |V\rangle)$. We define the spin-photon coincidence probability as $C_{ij} = p_{ij}/\eta$, where η denotes the PSB detection probability when the spin is fully in $|\uparrow\rangle$, p_{ij} denotes the joint coincident probability of PSB and ZPL, with a subscript i referring to the spin state and a

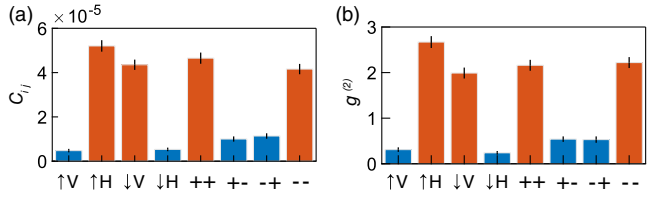

FIG. 3. Coincidence and cross-correlations of the spin-photon entanglement. (a) Coincidence results. (b) Cross-correlations. Both measurements are performed in the eigenbasis and superpositional basis.

subscript j referring to the photon state. The results are given in Fig. 3(a). To evaluate the entanglement, we first measure the visibility in the eigenbasis, which is defined as

$$V_e = \frac{C_{\uparrow H} + C_{\downarrow V} - C_{\uparrow V} - C_{\downarrow H}}{C_{\uparrow H} + C_{\downarrow V} + C_{\uparrow V} + C_{\downarrow H}}, \tag{1}$$

and get the result of $V_e = 81.0\% \pm 3.4\%$. Afterward, we perform measurement in the superpositional basis. For the photonic state, this is achieved by rotating the half-wave plate in Fig. 2(a). For the spin state, this is achieved via adding a $\pi/2$ or $3\pi/2$ pulse using MW_2. By using a similar definition, we get the superpositional visibility as $V_s = 60.9\% \pm 3.5\%$. From these two visibilities, we can estimate the entanglement fidelity as $F \approx (1 + V_e + 2V_s)/4 = 75.7\% \pm 1.5\%$, by assuming similar visibilities for the two superpositional bases [36]. The result is significant higher than the bound of 50% to certify entanglement.

Multiple factors contribute to infidelity of the spin-photon entanglement. The dominant cause is the spin flips during nonradiative decay. During the early excitation in Fig. 1(a), the spin has a change of 50% to decay through the MS levels in Fig. 1(b). Further decay from the MS levels will result in spin flips. Since the interval between the early excitation and the late excitation is much longer then the MS lifetime, the spin flips will result in some additional incoherent terms. This mechanism explains why we observe more coincidence counts for $C_{\uparrow H}$ than $C_{\downarrow V}$. These additional counts in $C_{\uparrow H}$ also reduce the visibility in the superpositional basis partially since these terms decay through nonradiative channels and are incoherent [30]. For our current experiment, we estimate that this mechanism will result in a maximal fidelity of 90%. We would like to note that this limitation will be mitigated significantly if we make use of the V2 defect instead. In this situation, the larger zero-field splitting (70 MHz) allows using a MW π pulse that is much shorter than the MS lifetime. Accordingly to our estimation [30], a fidelity as high as 98.1% can be achieved.

In contrast to the entanglement generation process in an ensemble system [37], the spin-photon entanglement generation process is in principle deterministic, albeit the emitted photon has a limited efficiency of lying in ZPL and being collected. This deterministic feature is verified via measuring the photonics cross-correlation $g^{(2)}$ between the ZPL and the PSB. Its definition is $g^{(2)}_{ij} = p_{ij}/p_i p_j$, where p_i denotes the PSB detection probability, p_j denotes the ZPL detection probability. For a pair of ideal deterministic spin-photon entanglement, $g^{(2)} \simeq 2$ for $|\uparrow\rangle|H\rangle$, $|\downarrow\rangle|V\rangle$, $|+\rangle|+\rangle$, and $|-\rangle|-\rangle$ that are named as high terms; while $g^{(2)} \simeq 0$ for $|\uparrow\rangle|V\rangle$, $|\downarrow\rangle|H\rangle$, $|+\rangle|-\rangle$, and $|-\rangle|+\rangle$ that named as low terms. The measured results are shown in Fig. 3(b). The average $g^{(2)}$ for the high terms is 2.26 ± 0.06, which is slightly higher than the theoretical value. We think it is due to instability of the charge state and the optical transition frequency, causing the V1 defect to have a minor chance to escape from being manipulated by the optical pulses and contributing to photon counts, which will lead to an increase of $g^{(2)}$ for the high terms as a result.

The entanglement generation probability is established to be 2×10^{-4} [30], defined as the probability to get a ZPL photon in a single mode fiber. The probability can be enhanced by incorporating the spin into nanocavities, which are coupled to on-chip waveguides [38]. Efficient collection can be achieved with tapered-fiber waveguide coupling. As a 1D photonic crystal cavity with quality factor of 2×10^4 in this work [26], the cavity coupling to single spin have a maximum Purcell factor of $F \sim 134$. In this case, the Debye-Waller factor (η_d) will be improved from 8% to 92% and the quantum efficiency (η_q) will be improved from 50% to 92%. Taking into account the coupling loss to the feeding waveguide, the on-resonance transmission η_t of the fundamental cavity mode can be achieved to 94% according to this work [38]. With the same manner of tapered-fiber waveguide coupling in this work [13], the coupling efficiency η_c can be achieved to 93%. The overall entanglement generation probability can be improved to $\eta = \eta_d \eta_q \eta_t \eta_c = 74\%$.

In conclusion, we report the first experimental demonstration of spin-photon entanglement in silicon carbide, which is enabled by stable and narrow optical transitions, high-fidelity spin manipulation, and phase coherent dual-step optical excitations. With two pairs of such spin-photon entanglement it is straightforward to entangle two remote nodes via entanglement swapping [39,40]. Fidelity of the spin-photon entanglement can be further improved significantly by making use of a MW π pulse that is much shorter than the lifetime of the metastable states. The entanglement generation rate can be further improved significantly via fabricating state-of-the-art photonic nanostructures around the defect [26,27,27] and harnessing high-efficient adiabatic coupling with a tapered fiber [38]. For long-lived storage, one can make use of the ^{29}Si nuclear spin with recently demonstrated coherent control over individual nuclear spins and electron-nuclear spin pair with high fidelity [25]. By making the transition from electrical spin to nuclear, a long-lived spin-photon entanglement will be

foreseeable in the very near future. By utilizing the nonlinearity of 4H-SiC, on-chip wavelength conversion to the telecom band can be implemented, which leads to ultracompact chip-based integration. Based on these improvements, the silicon vacancy defect in SiC may become a very promising approach for quantum networks.

This research was supported by the Innovation Program for Quantum Science and Technology (No. 2021ZD 0301103), National Natural Science Foundation of China, and the Chinese Academy of Sciences.

[*]These authors contributed equally to this work.

[1] H. J. Kimble, The quantum internet, Nature (London) **453**, 1023 (2008).
[2] S. Wehner, D. Elkouss, and R. Hanson, Quantum internet: A vision for the road ahead, Science **362**, eaam9288 (2018).
[3] H.-J. Briegel, W. Dür, J. I. Cirac, and P. Zoller, Quantum repeaters: The role of imperfect local operations in quantum communication, Phys. Rev. Lett. **81**, 5932 (1998).
[4] N. Sangouard, C. Simon, H. de Riedmatten, and N. Gisin, Quantum repeaters based on atomic ensembles and linear optics, Rev. Mod. Phys. **83**, 33 (2011).
[5] X.-J. Wang, S.-J. Yang, P.-F. Sun, B. Jing, J. Li, M.-T. Zhou, X.-H. Bao, and J.-W. Pan, Cavity-Enhanced atom-photon entanglement with subsecond lifetime, Phys. Rev. Lett. **126**, 090501 (2021).
[6] D. D. Awschalom, R. Hanson, J. Wrachtrup, and B. B. Zhou, Quantum technologies with optically interfaced solid-state spins, Nat. Photonics **12**, 516 (2018).
[7] P. Lodahl, S. Mahmoodian, and S. Stobbe, Interfacing single photons and single quantum dots with photonic nanostructures, Rev. Mod. Phys. **87**, 347 (2015).
[8] L. Robledo, L. Childress, H. Bernien, B. Hensen, P. F. Alkemade, and R. Hanson, High-fidelity projective read-out of a solid-state spin quantum register, Nature (London) **477**, 574 (2011).
[9] B. Hensen, H. Bernien, A. E. Dréau, A. Reiserer, N. Kalb, M. S. Blok, J. Ruitenberg, R. F. Vermeulen, R. N. Schouten, C. Abellán *et al.*, Loophole-free bell inequality violation using electron spins separated by 1.3 kilometres, Nature (London) **526**, 682 (2015).
[10] M. Ruf, N. H. Wan, H. Choi, D. Englund, and R. Hanson, Quantum networks based on color centers in diamond, J. Appl. Phys. **130**, 070901 (2021).
[11] M. Pompili, S. L. Hermans, S. Baier, H. K. Beukers, P. C. Humphreys, R. N. Schouten, R. F. Vermeulen, M. J. Tiggelman, L. dos Santos Martins, B. Dirkse *et al.*, Realization of a multinode quantum network of remote solid-state qubits, Science **372**, 259 (2021).
[12] S. Hermans, M. Pompili, H. Beukers, S. Baier, J. Borregaard, and R. Hanson, Qubit teleportation between non-neighbouring nodes in a quantum network, Nature (London) **605**, 663 (2022).
[13] M. K. Bhaskar, R. Riedinger, B. Machielse, D. S. Levonian, C. T. Nguyen, E. N. Knall, H. Park, D. Englund, M. Lončar, D. D. Sukachev *et al.*, Experimental demonstration of memory-enhanced quantum communication, Nature (London) **580**, 60 (2020).
[14] P.-J. Stas, Y. Q. Huan, B. Machielse, E. N. Knall, A. Suleymanzade, B. Pingault, M. Sutula, S. W. Ding, C. M. Knaut, D. R. Assumpcao *et al.*, Robust multi-qubit quantum network node with integrated error detection, Science **378**, 557 (2022).
[15] M. Atatüre, D. Englund, N. Vamivakas, S.-Y. Lee, and J. Wrachtrup, Material platforms for spin-based photonic quantum technologies, Nat. Rev. Mater. **3**, 38 (2018).
[16] G. Zhang, Y. Cheng, J.-P. Chou, and A. Gali, Material platforms for defect qubits and single-photon emitters, Appl. Phys. Rev. **7**, 031308 (2020).
[17] G. Wolfowicz, F. J. Heremans, C. P. Anderson, S. Kanai, H. Seo, A. Gali, G. Galli, and D. D. Awschalom, Quantum guidelines for solid-state spin defects, Nat. Rev. Mater. **6**, 906 (2021).
[18] N. T. Son, C. P. Anderson, A. Bourassa, K. C. Miao, C. Babin, M. Widmann, M. Niethammer, J. Ul Hassan, N. Morioka, I. G. Ivanov, F. Kaiser, J. Wrachtrup, and D. D. Awschalom, Developing silicon carbide for quantum spintronics, Appl. Phys. Lett. **116**, 190501 (2020).
[19] D. M. Lukin, M. A. Guidry, and J. Vučković, Integrated quantum photonics with silicon carbide: Challenges and prospects, PRX Quantum **1**, 020102 (2020).
[20] R. Nagy, M. Niethammer, M. Widmann, Y.-c. Chen, P. Udvarhelyi, C. Bonato, J. U. Hassan, R. Karhu, I. G. Ivanov, N. T. Son, J. R. Maze, T. Ohshima, Ö. O. Soykal, Á. Gali, S.-y. Lee, F. Kaiser, and J. Wrachtrup, High-fidelity spin and optical control of single silicon-vacancy centres in silicon carbide, Nat. Commun. **10**, 1954 (2019).
[21] C. P. Anderson, A. Bourassa, K. C. Miao, G. Wolfowicz, P. J. Mintun, A. L. Crook, H. Abe, J. Ul Hassan, N. T. Son, T. Ohshima *et al.*, Electrical and optical control of single spins integrated in scalable semiconductor devices, Science **366**, 1225 (2019).
[22] H. B. Banks, Ö. O. Soykal, R. L. Myers-Ward, D. K. Gaskill, T. L. Reinecke, and S. G. Carter, Resonant optical spin initialization and readout of single silicon vacancies in 4H-SiC, Phys. Rev. Appl. **11**, 024013 (2019).
[23] A. Bourassa, C. P. Anderson, K. C. Miao, M. Onizhuk, H. Ma, A. L. Crook, H. Abe, J. Ul-Hassan, T. Ohshima, N. T. Son *et al.*, Entanglement and control of single nuclear spins in isotopically engineered silicon carbide, Nat. Mater. **19**, 1319 (2020).
[24] N. Morioka *et al.*, Spin-controlled generation of indistinguishable and distinguishable photons from silicon vacancy centres in silicon carbide, Nat. Commun. **11**, 2516 (2020).
[25] C. Babin *et al.*, Fabrication and nanophotonic waveguide integration of silicon carbide colour centres with preserved spin-optical coherence, Nat. Mater. **21**, 67 (2021).
[26] D. M. Lukin, C. Dory, M. A. Guidry, K. Y. Yang, S. D. Mishra, R. Trivedi, M. Radulaski, S. Sun, D. Vercruysse, G. H. Ahn, and J. Vučković, 4H-silicon-carbide-on-insulator for integrated quantum and nonlinear photonics, Nat. Photonics **14**, 330 (2020).
[27] A. L. Crook, C. P. Anderson, K. C. Miao, A. Bourassa, H. Lee, S. L. Bayliss, D. O. Bracher, X. Zhang, H. Abe, T. Ohshima *et al.*, Purcell enhancement of a single silicon

carbide color center with coherent spin control, Nano Lett. **20**, 3427 (2020).

[28] D. M. Lukin, M. A. Guidry, J. Yang, M. Ghezellou, S. Deb Mishra, H. Abe, T. Ohshima, J. Ul-Hassan, and J. Vučković, Two-emitter multimode cavity quantum electrodynamics in thin-film silicon carbide photonics, Phys. Rev. X **13**, 011005 (2023).

[29] C. P. Anderson, E. O. Glen, C. Zeledon, A. Bourassa, Y. Jin, Y. Zhu, C. Vorwerk, A. L. Crook, H. Abe, J. Ul-Hassan, T. Ohshima, N. T. Son, G. Galli, and D. D. Awschalom, Five-second coherence of a single spin with single-shot readout in silicon carbide, Sci. Adv. **8**, eabm5912 (2022).

[30] See Supplemental Material at http://link.aps.org/supplemental/10.1103/PhysRevLett.132.160801 for a detailed description of our sample preparation, basic characterization, and theoretical analysis about the infidelity and entanglement generation probability.

[31] A. Tchebotareva, S. L. N. Hermans, P. C. Humphreys, D. Voigt, P. J. Harmsma, L. K. Cheng, A. L. Verlaan, N. Dijkhuizen, W. de Jong, A. Dréau, and R. Hanson, Entanglement between a diamond spin qubit and a photonic time-bin qubit at telecom wavelength, Phys. Rev. Lett. **123**, 063601 (2019).

[32] M. H. Appel, A. Tiranov, S. Pabst, M. L. Chan, C. Starup, Y. Wang, L. Midolo, K. Tiurev, S. Scholz, A. D. Wieck, A. Ludwig, A. S. Sørensen, and P. Lodahl, Entangling a hole spin with a time-bin photon: A waveguide approach for quantum dot sources of multiphoton entanglement, Phys. Rev. Lett. **128**, 233602 (2022).

[33] H. Bernien, B. Hensen, W. Pfaff, G. Koolstra, M. S. Blok, L. Robledo, T. H. Taminiau, M. Markham, D. J. Twitchen, L. Childress, and R. Hanson, Heralded entanglement between solid-state qubits separated by three meters, Nature **497**, 86 (2013).

[34] A. Nick Vamivakas, Y. Zhao, C.-Y. Lu, and M. Atatüre, Spin-resolved quantum-dot resonance fluorescence, Nat. Phys. **5**, 198 (2009).

[35] C.-W. Yang, Y. Yu, J. Li, B. Jing, X.-H. Bao, and J.-W. Pan, Sequential generation of multiphoton entanglement with a Rydberg superatom, Nat. Photonics **16**, 658 (2022).

[36] O. Gühne and G. Tóth, Entanglement detection, Phys. Rep. **474**, 1 (2009).

[37] A. Kuzmich, W. Bowen, A. Boozer, A. Boca, C. Chou, L.-M. Duan, and H. Kimble, Generation of nonclassical photon pairs for scalable quantum communication with atomic ensembles, Nature (London) **423**, 731 (2003).

[38] A. Sipahigil, R. E. Evans, D. D. Sukachev, M. J. Burek, J. Borregaard, M. K. Bhaskar, C. T. Nguyen, J. L. Pacheco, H. A. Atikian, C. Meuwly *et al.*, An integrated diamond nanophotonics platform for quantum-optical networks, Science **354**, 847 (2016).

[39] J.-W. Pan, D. Bouwmeester, H. Weinfurter, and A. Zeilinger, Experimental entanglement swapping: Entangling photons that never interacted, Phys. Rev. Lett. **80**, 3891 (1998).

[40] J.-W. Pan, Z.-B. Chen, C.-Y. Lu, H. Weinfurter, A. Zeilinger, and M. Żukowski, Multiphoton entanglement and interferometry, Rev. Mod. Phys. **84**, 777 (2012).